DOI: 10.24874/ti.2055.10.25.01

Tribology in Industry

www.tribology.rs

RESEARCH

Greenly Synthesized Lilium candidum L.-Derived Silver Nanoparticles as Sustainable Corrosion Inhibitors and Surface Protectants for Industrial Applications

Rabab M. Nasser[a,*]

[a]*Petroleum Applications Department, Egyptian Petroleum Research Institute, Nasr City, Cairo, Egypt.*

Keywords:

Silver nanoparticles (AgNPs)
Green synthesis
Lilium candidum L.
Corrosion inhibition
Antifungal activity
Sustainable materials
Surface protection
Industrial applications

* Corresponding author:

Rabab M. Nasser
E-mail: rabab_nasser@yahoo.com

Received: 28 October 2025
Revised: 19 December 2026
Accepted: 30 January 2026

A B S T R A C T

This study explores a green, sustainable method for synthesizing silver nanoparticles (AgNPs) using ethanolic extracts from Lilium candidum L. leaves (LL), stems (SL), and flowers (ZL), which serve as natural reducing and stabilizing agents. Characterization via UV–Vis, FTIR, XRD, DLS, and TEM confirmed the formation of spherical AgNPs (20–60 nm) with a face-centered cubic structure. The biosynthesized AgNPs displayed significant antifungal activity against Aspergillus niger, A. flavus, and A. fumigatus, with inhibition zones reaching 27 ± 1.5 mm at 250 µg/mL. Additionally, corrosion inhibition studies on mild steel in 3.5 wt.% NaCl revealed that efficiency (IE%) depends on inhibitor type, concentration, and immersion time. At 0.03 g/L after 24 hours, crude extracts showed IE% values of 80% (LL), 73% (SL), and 67% (ZL). Their AgNPs derivatives significantly enhanced performance, achieving 94.7% (L-AgNPs), 93.3% (S-AgNPs), and 89.23% (Z-AgNPs). Protection improved with higher concentrations until surface saturation but gradually decreased over prolonged exposure (24–72 hours). The adsorption process followed the Langmuir isotherm, suggesting a spontaneous and predominantly physisorptive interaction between the inhibitors and the metal surface. These results highlight the dual potential of L. candidum-mediated AgNPs as potent antifungal agents and high-efficiency corrosion inhibitors.

© 2026 Published by Faculty of Engineering

Article in Press

1. INTRODUCTION

In many industrial sectors, mild steel corrosion is still a serious issue that frequently leads to structural degradation, safety risks, and significant financial costs. Understanding the causes of corrosion and creating workable preventative measures are necessary to extend the life of industrial systems and reduce maintenance costs. One of the most crucial defense strategies for lowering metal deterioration is the use of corrosion inhibitors, both organic and inorganic.

Organic inhibitors made from natural sources are gaining attention for their environmental friendliness, while inorganic inhibitors are valued for their strong and reliable protection. The use of hybrid organic-inorganic inhibitors is an interesting tactic that combines the benefits of both systems [1-7]. Because of their remarkable surface reactivity, capacity to form barriers, and innate antibacterial qualities, silver nanoparticles (AgNPs) have garnered a lot of attention and are useful for a variety of corrosion prevention applications. Using plant extracts as natural reducing and stabilizing agents is one of the most sustainable methods for their production. In addition to reducing silver ions to metallic silver, phytochemicals such flavonoids, phenols, terpenoids, and proteins stabilize the resultant nanoparticles and stop them from aggregating. This green synthesis method eliminates dangerous chemicals and high-energy procedures while being economical and eco-friendly [8,9].

The Madonna lily, or Lilium candidum L., is an attractive plant that is common to the Mediterranean region, especially Southern Turkey. Beyond its aesthetic appeal, Lilium candidum yields a variety of bioactive substances, such as flavonoids, alkaloids, and saponins, which have been utilized in traditional medicine to heal burns, ulcers, and wounds. Its potential as a natural source of beneficial phytochemicals has been highlighted by recent research that has proven a number of its biological properties, including hepatoprotective, antiviral, and anti-tumor actions [10-16]. A variety of plants, such as Polyalthia longifolia, Citrus sinensis, Ocimum sanctum, Aloe vera, and Moringa oleifera [13,14,17-20] have been successfully used for AgNP synthesis, with the resulting nanoparticles characterized by techniques such as UV–visible spectroscopy, FTIR, SEM, TEM, and XRD [15,21,22]. These plant-based AgNPs exhibit a broad spectrum of biological activities, including antibacterial, antifungal, antiviral, anti-inflammatory, and anticancer effects, making them useful for wound healing, drug delivery, and biomedical coatings [10-12].

Despite green synthesis of AgNPs using plant extracts has been extensively investigated, the application of Lilium candidum L.-derived AgNPs as dual-function corrosion inhibitors and antifungal agents is yet understudied. Previous research has concentrated on either solitary application (corrosion or antifungal characteristics) rather than their synergistic combination. Furthermore, our understanding of how Lilium-derived phytochemicals promote nanoparticle production and surface protection is limited. This study fills these gaps by fully characterizing Lilium AgNPs and establishing their superior dual functionality.

The main objective of this study is to synthesize AgNPs from Lilium candidum L. extracts utilizing ecologically friendly green chemistry techniques. Characterization of the prepared extracts and its AgNPs using spectroscopic and microscopic techniques. The antifungal activity against Aspergillus species was Assessed. The corrosion inhibition mechanisms were evaluated by electrochemical investigations, and adsorption modelling. Quantum chemical calculations were performed to explain inhibitor activity.

2. MATERIALS AND METHODS

2.1 Materials

Fresh Lilium candidum L. plants were obtained from Samtah, Jazan, Saudi Arabia. Analytical-grade ethanol (70%) and silver nitrate ($AgNO_3$, 99.8%, Chem Lab, Belgium) were used for the experiments. All chemicals and reagents were used as received without further purification.

2.2 Plant extract preparation and phytochemical screening.

Approximately 100 g of Lilium candidum L. (leaf, stem, and flower) were washed, chopped into small pieces, and air-dried. The dried material was ground into a coarse powder using an electric grinder. Each portion (leaves, stems, and flowers) was placed in a separate glass jar, and 500 mL of 70% ethanol was added as solvent to ensure complete submersion. The mixtures were kept in a cool, dark place for seven days to allow extraction. Afterwards, the contents were filtered through Whatman No. 1 filter paper, and the filtrates were stored in airtight containers for further analysis.

The ethanolic extracts were qualitatively analyzed for major phytochemical constituents following standard methods. Flavonoids were

Article in Press

confirmed by green-to-blue-black coloration upon addition of ferric chloride solution. Alkaloids were detected by mixing the extract with chloroform and treating with Mayer's or Dragendorff's reagent, producing characteristic white precipitate. Terpenoids were identified by evaporating the extract, gently heating with concentrated sulfuric acid, and observing violet coloration in the lower layer. Phenolic compounds were identified by dark green color development after sodium hydroxide treatment. Tannins were verified by white or blue-black precipitate formation with ferric chloride or lead acetate. Reducing sugars were confirmed by orange precipitate with Fehling's or Benedict's reagents. Starch was indicated by purple coloration with iodine solution [23].

2.3 Silver nanoparticles synthesis

Silver nanoparticles (AgNPs) were synthesized by adding 0.3 g of $AgNO_3$ to 50 mL of the respective plant extract under continuous stirring at 50-60°C for 4 hours. The formation of brown coloration indicated successful reduction of Ag^+ ions to metallic AgNPs. Synthesis was performed in triplicate (n = 3) to ensure reproducibility.

2.4 Nanoparticles characterization.

The optical properties of synthesized AgNPs were analyzed using a UV-visible spectrophotometer (Model 6800). The surface plasmon resonance (SPR) peak confirmed nanoparticle formation and was used to monitor synthesis efficiency.

FTIR spectra of both the extracts and their corresponding AgNPs were recorded (4000-400cm^{-1}) using a Thermo Scientific Nicolet spectrometer with KBr pellets. Dried powder samples were used to identify functional groups responsible for capping and stabilization of the nanoparticles. Peak assignments follow standard spectroscopic conventions and are clearly labeled in Figure 1.

Zeta potential measurements were carried out using a Zetasizer Nano Series (Malvern Instruments) to assess surface charge and colloidal stability of L-AgNPs, S-AgNPs, and Z-AgNPs. Samples were diluted with Milli-Q water and analyzed in folded capillary cells under an applied electric field. Electrophoretic mobility was converted to zeta potential values using the Smoluchowski equation, with higher absolute values indicating greater colloidal stability.

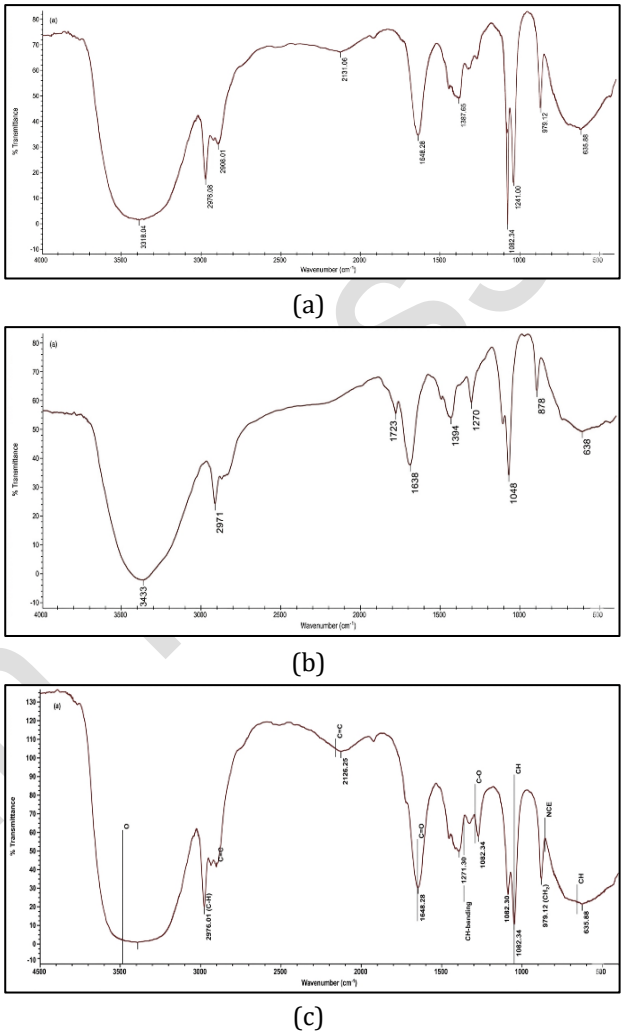

Fig. 1. FT-IR spectrum of lilium candidum L. (a) for LL extract, (b) for SL extract, and (c) for ZL extract.

The hydrodynamic diameter and size distribution of nanoparticles were determined by DLS. Scattered light intensity was analyzed using the Stokes-Einstein equation to estimate particle size uniformity and dispersion stability. Polydispersity index (PDI) values were calculated to assess size distribution homogeneity.

The crystalline nature phases of AgNPs were were determined by XRD using a Bruker D8 Advance diffractometer with Cu-Kα radiation (λ = 0.1544 nm) across a 2θ range of 10-90°, following ASTM B921 standards. Crystalline phases were determined and indexed to face-centered cubic (FCC) silver structures.

Article in Press

Morphological features and particle size were examined using a JEOL JEM-100 CXI transmission electron microscope operating at 100 kV. TEM samples were prepared by drop-casting AgNPs suspension onto carbon-coated copper grids and air-drying at room temperature.

Stability Studies for AgNP suspensions were done by storing at 4°C in dark glass bottles. UV-Vis spectra were recorded at 0, 7, 14, 21, and 28 days. No color change or precipitation was observed, confirming excellent long-term stability.

2.5 Antifungal activity

Fungal strains (Aspergillus niger, A. flavus, and A. fumigatus) were cultured and maintained on Czapek's agar by repeated sub-culturing. Antifungal activity of synthesized AgNPs was evaluated using the agar well diffusion technique. Inoculated agar plates were prepared by spreading fungal spores over the surface, and wells (6 mm diameter) were made using a sterile cork borer. Defined volumes of AgNPs suspensions (250 µg/mL) were added to the wells in triplicate, and plates were incubated at 37°C for 24 hours. Inhibition zones were measured in millimeters to determine antifungal potency (n = 3, Mean ± SD reported) [24].

2.6 Corrosion inhibition studies

Commercial mild steel (composition: Fe 99%, C 0.312%, Si 0.193%, Mn 0.922%, P 0.010%, S 0.008%, Cr 0.21%) was cut into rectangular specimens (10 × 2 × 0.2 cm). The surfaces were polished sequentially with emery papers (800–2000 grit), cleaned with acetone and deionized water, and air-dried before testing. All measurements were performed in triplicate (n=3).

Polished steel coupons were immersed in 3.5 wt. % NaCl solution with and without varying concentrations (0.03 – 0.0025g/L) of AgNPs inhibitors for 24–72 hours at room temperature25±2˚C. After immersion, samples were washed with distilled water, dried, and reweighed. All measurements were performed in triplicate to ensure reproducibility [25,26]. Weight loss (ΔW), corrosion rate (CR) and inhibition efficiency (IE%) were calculated using equations (1-4):

$$\Delta W = W1 - W2 \quad (1)$$

$$CR = \frac{\Delta W}{At} \quad (2)$$

$$\theta = \frac{(CRblank - CRinh)}{CRblank} \quad (3)$$

$$IE\% = \theta * 100 \quad (4)$$

Where ΔW is the weight loss, A is the exposed surface area, t is immersion time, and CR_{blank} and CR_{inh} are the corrosion rates in the absence and presence of inhibitors, respectively. Θ is surface coverage, ASTM G-31 [27].

Electrochemical experiment, ASTM G-59 [28] were performed using a CHI660D workstation with a standard three-electrode setup [29]: mild steel as the working electrode (1 cm^2 area), Ag/AgCl as reference, and platinum as counter electrode. Tests were conducted in 3.5 wt.% NaCl solution containing various concentrations (0.0025-0.03 g L^{-1}) of LL, SL, ZL, and their AgNPs derivatives. Open-circuit potential (OCP) was monitored for 3600 s, followed by potentiodynamic polarization from –0.5 V to +0.5 V at a 0.5 mV s^{-1} scan rate. Inhibition efficiency and polarization resistance were calculated using standard electrochemical equations [30,31]. Cyclic voltammetry was performed to evaluate cathodic and anodic reaction kinetics.

Adsorption behavior was analysed at 60˚C ≈ 333K, using the Langmuir isotherm model, equation (5):

$$\frac{C}{\theta} = \frac{1}{kads} + C \quad (5)$$

Where C is inhibitor concentration (g/L), θ is surface coverage, and K_{ads} is the adsorption equilibrium constant. Langmuir plots were generated, and R^2 values confirmed model validity.

Initial geometry optimization was performed using ChemDraw 3D software. Electronic structure and reactivity parameters of the main phytochemicals were calculated using B3LYP/6-311G basis set (industry standard for organic compounds). Parameters calculated include: Energy gap (ΔE, eV), Ionization Potential (IP, eV), Electron Affinity (EA, eV), Electronegativity (χ, eV), Chemical Hardness (η, eV), and Chemical Softness (σ, eV). Structural formulas for all compounds and their parameters relevance to corrosion inhibition was explained in the Discussion section.

Article in Press

3. RESULTS AND DISSCUSIONS

Table 1, summarizes the designations and compositions of the prepared extracts and their corresponding AgNPs.

Phytochemical screening, Table 2, revealed the presence of flavonoids, alkaloids, terpenoids, phenols, tannins, reducing sugars, and starch across all three plant parts, with varying abundance levels. These compounds served as both reducing and stabilizing agents during synthesis [32].

Table 1. Designation of the prepared extracts and their AgNPs.

Plant part	Extract	Designation	Nano Particles	Designation
Leaf	L– Lilium	LL	AgNPs from leaf extract	L-AgNPs
Stem	S-Lilium	SL	AgNPs from stem extract	S-AgNPs
Flower	Z-Lilium	ZL	AgNPs from flower extract	Z-AgNPs

Table 2. Phytochemical compounds in lilium candidum L. extracts.

Test for	LL	SL	ZL
Flavonoids	+++	+++	+++
Alkaloids	+++	+++	+++
Terpenoids	++	++	+++
Phenol	+++	+++	+++
Tannins	+	+	+
Reducing sugars	++	+	+
Starch	+	+	+

+++ major abundance, ++ moderate abundance, and + rarely abundance

FTIR spectroscopy, Figure 1, confirmed functional groups related to the three plant extracts. The leaf extract displayed strong O-H stretching around 3410 cm^{-1}, hydroxyl groups and C=O stretching near 1640 cm^{-1} which may be related to phenolic/flavonoid compounds. The stem extract showed carbonyl groups at 1723cm^{-1} and alkyne/nitrile functionality at 2131 cm^{-1}. The flower extract exhibited similar O-H features with additional C-O stretching around 1044 cm^{-1}. These spectral variations suggest differences in phytochemical composition that influence antifungal and corrosion inhibition performance [33].

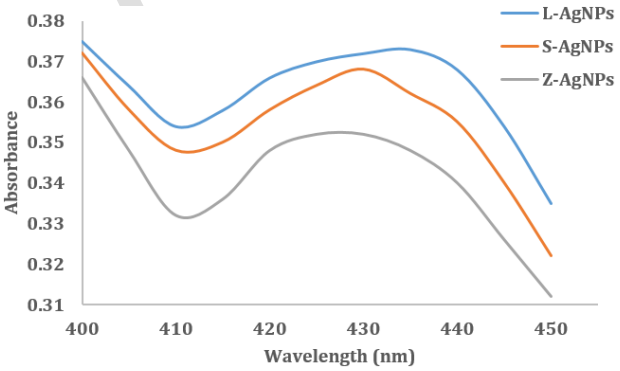

Fig. 2. AgNPs of lilium candidum L. extracts at 50-60˚C.

The UV-Vis spectra, Figure 2 revealed Surface Plasmon Resonance (SPR) peaks at approximately 410-440 nm, confirming AgNP formation. The slight shift in peak positions across leaf, stem, and flower extracts reflects differences in nanoparticle size and capping efficiency. Leaf-derived AgNPs (L-AgNPs) showed smallest peak shift, indicating more uniform size distribution and stable synthesis.

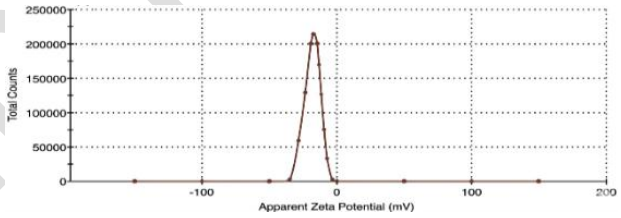

(a)

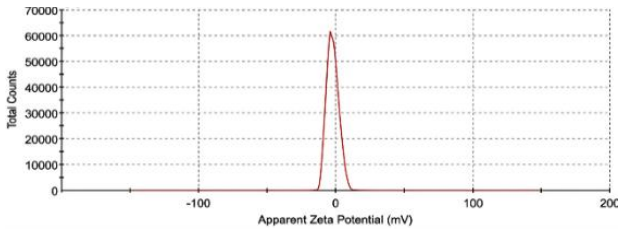

(b)

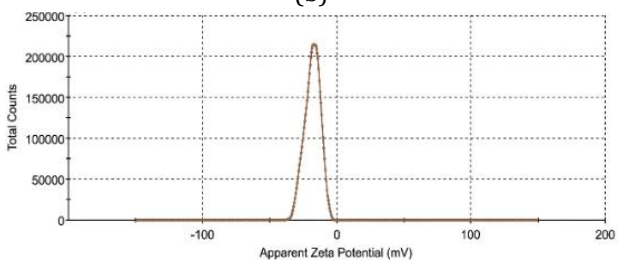

(c)

Fig. 3. Zeta potential of (a) L-AgNPs, (b) S-AgNPs, and (c) Z-AgNPs.

The most common phytochemical compounds in Lilium Candidum L. were detected by [12]. I)Jatrophan, II) 5-hydroxy-3-methyl-1-(3-methyl-

Article in Press

2-oxo-3-pyrroline-5-yl)-3-pyrroline-2-on, III) 5,5-oxydi-(3-methyl-3-pyroline-2-on), IV) kaempferol, V) (25S)-3β-{β-D-glucopyranosyl-(1→4)-[α-L-rhamnopyranosyl-(1→2)]-β-D-glucopyranosyloxy} spirost-5-ene-7-ol.

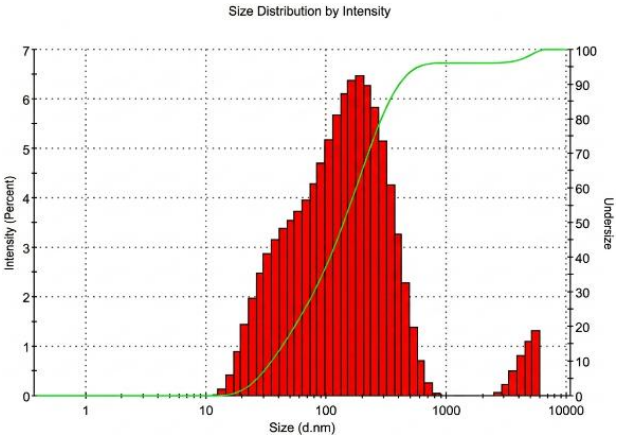

Fig. 4. DLS of lilium Z-AgNPs.

Dynamic light scattering (DLS) analysis revealed average hydrodynamic diameter (z-average) of approximately 92.47 nm for synthesized AgNPs, with polydispersity index (PDI) of 0.607, indicating moderately broad particle size distribution. Zeta potential analysis showed: L-AgNPs (-14.8 mV), S-AgNPs (-7.48 mV), and Z-AgNPs (-30 mV). The high negative potential of Z-AgNPs indicates superior colloidal stability, suggesting effective biomolecular capping [34,35] , Figures 3, 4.

X-ray diffraction patterns confirmed crystalline AgNPs with prominent peaks at 2θ ≈ 38.2° (111), 44.3° (200), 64.5° (220), and 78° (311) characteristic of face-centered cubic (FCC) silver crystal structure. A broad peak at 2θ ≈ 20° suggests residual organic matter or amorphous components from phytochemical capping, Figure 5.

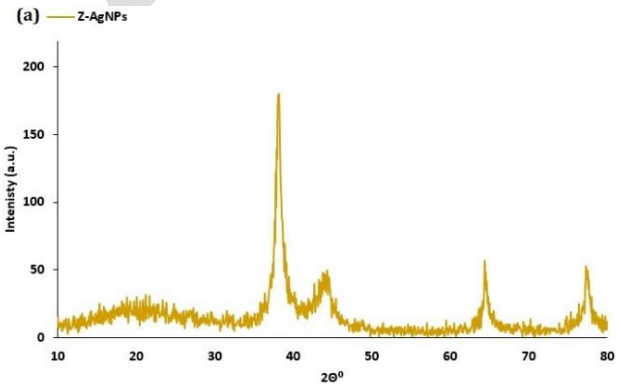

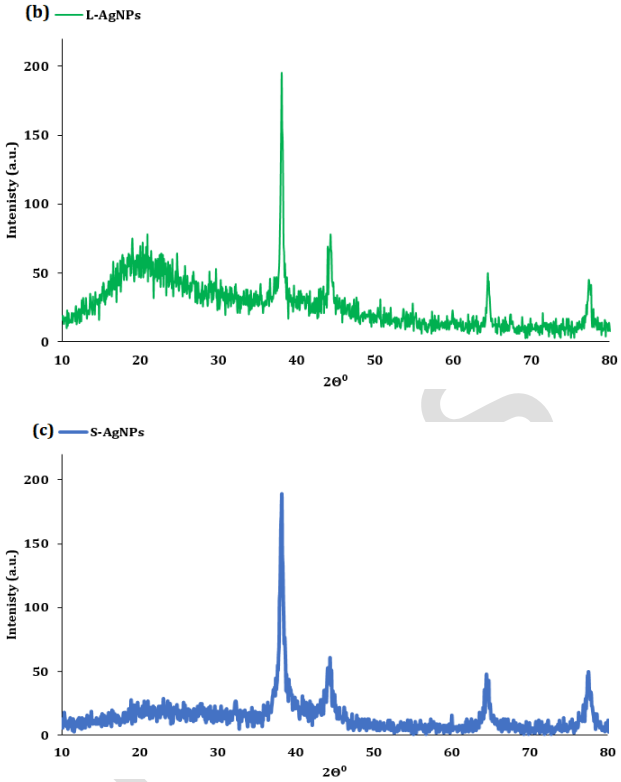

Fig. 5. XRD of lilium (a) S-AgNPs, (b) L-AgNPs, and (c) S-AgNPs.

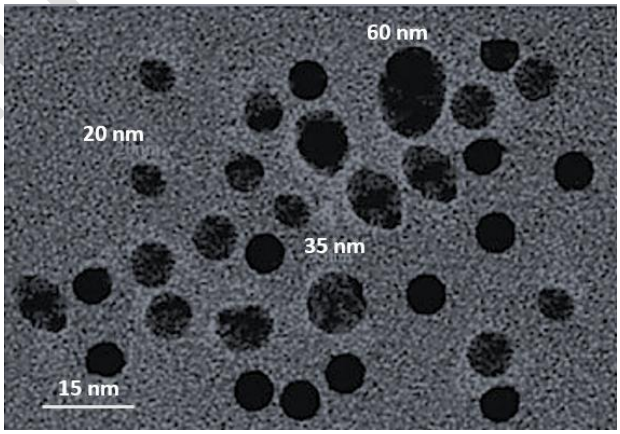

Fig. 6. TEM of lilium Z- AgNPs.

Antifungal testing using agar well diffusion method, Figure 7 revealed strong activity against Aspergillus species. At 250 µg/mL concentration, AgNPs produced inhibition zones of: A. niger (18 ± 1.2 mm), A. flavus (27 ± 1.5 mm), and A. fumigatus (21 ± 0.9 mm) (n=3, Mean ± SD). These results ($p < 0.05$, ANOVA) demonstrate significant antifungal potency, attributable to the nanoscale dimensions and high surface reactivity of AgNPs, which facilitate interaction with fungal cell walls and membranes, leading to structural disruption and growth inhibition.

Article in Press

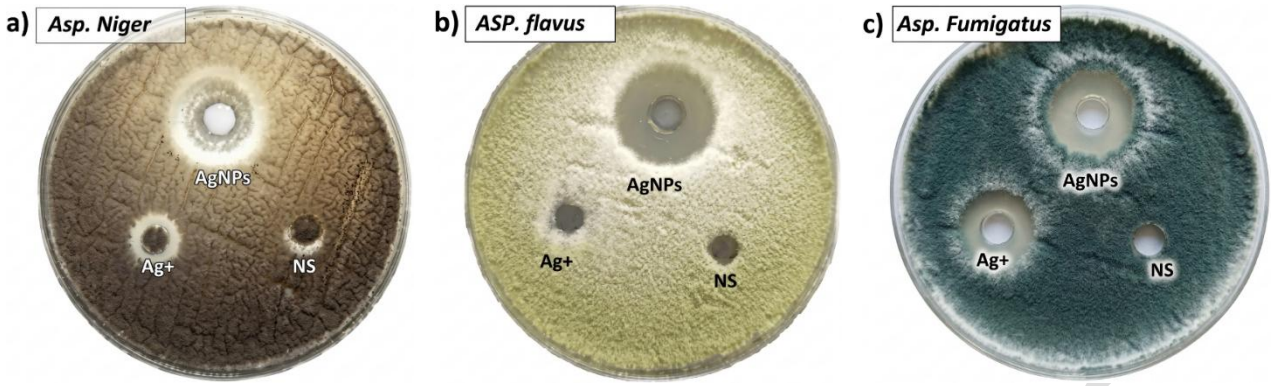

Fig 7. Antifungal effect of lilium Z-AgNPs using a) Asp. niger, b) Asp. flavus, and c) Asp. fumigatus.

Quantum chemical parameters, Table 3 provide insights into the electronic structure and reactivity of phytochemicals. Energy gap (ΔE) values ranged from 7.435-9.066 eV, with higher values indicating strong electron-donating ability and molecular stability. Compounds with narrower energy gaps exhibit greater chemical reactivity, facilitating efficient electron transfer for Ag^+ reduction and silver nanoparticle nucleation. Ionization Potential (IP) values reached 12.213 eV, reflecting the energy required for electron removal and molecular stability during metal-ligand interactions. Moderate electron affinity (EA) values (0.369-2.597 eV) indicate favorable capacity to accept electrons, enhancing coordination with silver ions and metallic surfaces, Figure 8.

Table 3. Quantum parameters of the isolated phytochemicals.

Compound	E_{HOMO} (eV)	E_{LUMO} E(eV)	ΔE (eV)	IP (eV)	EA (eV)	χ (eV)	η (eV)	S (eV^{-1})
Jatrophan	-12.213	-3.147	9.066	12.213	3.147	7.680	4.533	0.220
5-hydroxy-3-methyl-1-(3-methyl-2-oxo-3-pyrroline-5-yl)-3-pyrroline-2-on	-11.624	-2.899	8.725	11.624	2.899	7.262	4.362	0.229
5,5-oxydi-(3-methyl-3-pyroline-2-on)	-10.156	-2.721	7.435	10.156	2.721	6.439	3.718	0.269
kaempferol	-1.140	0.369	1.509	1.140	0.369	0.754	0.385	2.597
(25S)-3β-{β-D-glucopyranosyl-(1→4)-[α-L-rhamnopyranosyl-(1→2)]-β-D-glucopyranosyloxy} spirost-5-ene-7-ol	12.312	20.545	8.233	12.312	20.545	16.429	4.106	0.243

Electronegativity (χ) values demonstrate strong electron-attracting tendency, promoting stable adsorbed film formation. Chemical hardness (η) points to resistance toward electron density deformation, ensuring protective surface layer persistence. Chemical softness (σ) emphasizes adaptability and reactivity in metal ion bonding. Collectively, these quantum descriptors confirm that Lilium candidum phytochemicals are ideally suited for green synthesis of AgNPs and functioning as eco-friendly corrosion inhibitors.

Figures 9 and 10 illustrate the correlation between inhibition efficiency (IE%) and corrosion rate (CR) as a function of Lilium candidum L. extract and its silver nanoparticle (AgNPs) concentrations during mild steel corrosion tests. As presented in Tables 4 and 5, a clear trend emerges: increasing inhibitor concentration leads to a progressive rise in IE%, accompanied by a corresponding decline in CR. This behavior strongly indicates that higher concentrations of both the plant extract and its AgNPs enhance surface protection by reducing metal dissolution rates. The data presented in Figures 9 and 10 further confirm this observation, showing a substantial decrease in corrosion rate with increasing inhibitor concentration, alongside a consistent improvement in inhibition efficiency. This can be attributed to the adsorption of active phytochemical constituents and AgNPs onto the steel surface, forming a compact, adherent protective film that impedes corrosive attack. Beyond a certain concentration threshold, the inhibition efficiency tends to plateau, suggesting that surface saturation has been achieved and additional inhibitor no longer enhances protection.

Article in Press

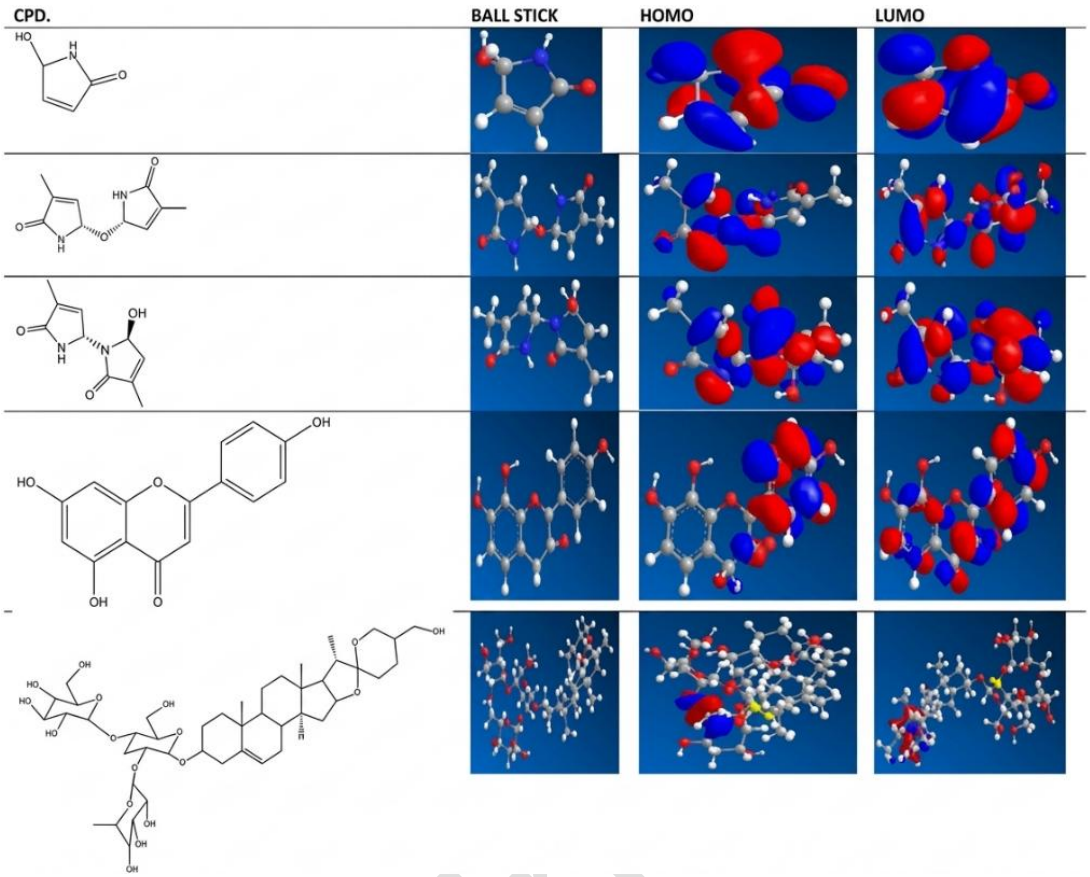

Fig. 8. HOMO and LUMO orbitals for the most abundant phytochemicals in lilium candidum L.

Table 4. Weight loss parameters of lilium candidum L extracts (24hr-72hr).

		After 24 hr.				
	Sample	Δw	At	CR	Θ	IE%
LL	0	0.15	5760.00	2.60E-05	0.00	0.00
	0.0025	0.09	5760.00	1.56E-05	0.40	40.00
	0.005	0.08	5760.00	1.39E-05	0.47	46.67
	0.01	0.07	5760.00	1.22E-05	0.53	53.33
	0.02	0.05	5760.00	8.68E-06	0.67	66.67
	0.03	0.03	5760.00	5.21E-06	0.80	80.00
SL	0.00	0.15	5760.00	2.60E-05	0.00	0.00
	0.0025	0.11	5760.00	1.91E-05	0.27	26.67
	0.0050	0.10	5760.00	1.74E-05	0.33	33.33
	0.01	0.08	5760.00	1.39E-05	0.47	46.67
	0.02	0.06	5760.00	1.04E-05	0.60	60.00
	0.03	0.04	5760.00	6.94E-06	0.73	73.33
ZL	0.00	0.15	5760.00	2.60E-05	0.00	0.00
	0.0025	0.12	5760.00	2.08E-05	0.20	20.00
	0.0050	0.11	5760.00	1.82E-05	0.30	30.00
	0.01	0.09	5760.00	1.56E-05	0.40	40.00
	0.02	0.07	5760.00	1.22E-05	0.53	53.33
	0.03	0.05	5760.00	8.68E-06	0.67	66.67

Article in Press

		After 48 hr.				
	Sample	Δw	At	CR	Θ	IE%
LL	0	0.35	11520.00	3.04E-05	0.00	0.00
	0.0025	0.22	11520.00	1.91E-05	0.37	37.14
	0.005	0.20	11520.00	1.74E-05	0.43	42.86
	0.01	0.17	11520.00	1.48E-05	0.51	51.43
	0.02	0.12	11520.00	1.04E-05	0.66	65.71
	0.03	0.10	11520.00	8.68E-06	0.71	71.43
SL	0.00	0.35	11520.00	3.04E-05	0.00	0.00
	0.0025	0.25	11520.00	2.17E-05	0.29	28.57
	0.0050	0.23	11520.00	2.00E-05	0.34	34.29
	0.01	0.18	11520.00	1.56E-05	0.49	48.57
	0.02	0.14	11520.00	1.22E-05	0.60	60.00
	0.03	0.12	11520.00	1.04E-05	0.66	65.71
ZL	0.00	0.35	11520.00	3.04E-05	0.00	0.00
	0.0025	0.26	11520.00	2.26E-05	0.26	25.71
	0.0050	0.24	11520.00	2.08E-05	0.31	31.43
	0.01	0.19	11520.00	1.65E-05	0.46	45.71
	0.02	0.15	11520.00	1.30E-05	0.57	57.14
	0.03	0.14	11520.00	1.22E-05	0.60	60.00

		After 72 hr.				
	Sample	Δw	At	CR	Θ	IE%
LL	0	0.45	17280	2.60E-05	0.00	0.00
	0.0025	0.30	17280	1.74E-05	0.33	33.33
	0.005	0.27	17280	1.56E-05	0.40	40.00
	0.01	0.23	17280	1.33E-05	0.49	48.89
	0.02	0.16	17280	9.26E-06	0.64	64.44
	0.03	0.14	17280	8.10E-06	0.69	68.89
SL	0.00	0.45	17280	2.60E-05	0.00	0.00
	0.0025	0.33	17280	1.91E-05	0.27	26.67
	0.0050	0.30	17280	1.74E-05	0.33	33.33
	0.01	0.26	17280	1.50E-05	0.42	42.22
	0.02	0.20	17280	1.16E-05	0.56	55.56
	0.03	0.16	17280	9.26E-06	0.64	64.44
ZL	0.00	0.45	17280	2.60E-05	0.00	0.00
	0.0025	0.35	17280	2.03E-05	0.22	22.22
	0.0050	0.32	17280	1.85E-05	0.29	28.89
	0.01	0.27	17280	1.56E-05	0.40	40.00
	0.02	0.22	17280	1.27E-05	0.51	51.11
	0.03	0.20	17280	1.16E-05	0.56	55.56

Article in Press

Table 5. Weight loss parameters of lilium candidium L AgNPs (24hr-72hr).

		After 24 hr.				
	Sample	Δw	At	CR	Θ	IE%
L-AgNPs	0	0.15	5760	2.6E-05	0	0
	0.0025	0.08	5760	1.4E-05	0.467	46.7
	0.005	0.06	5760	1E-05	0.6	60
	0.01	0.04	5760	6.9E-06	0.733	73.3
	0.02	0.02	5760	3.5E-06	0.867	86.7
	0.03	0.008	5760	1.4E-06	0.947	94.7
S-AgNPs	0.00	0.15	5760	2.6E-05	0	0
	0.0025	0.1	5760	1.7E-05	0.333	33.3
	0.0050	0.09	5760	1.6E-05	0.4	40
	0.01	0.07	5760	1.2E-05	0.533	53.3
	0.02	0.05	5760	8.7E-06	0.667	66.7
	0.03	0.01	5760	1.7E-06	0.933	93.3
Z-AgNPs	0.00	0.15	5760	2.6E-05	0	0
	0.0025	0.09	5760	1.6E-05	0.4	40
	0.0050	0.07	5760	1.2E-05	0.533	53.3
	0.01	0.05	5760	8.7E-06	0.667	66.7
	0.02	0.04	5760	6.9E-06	0.733	73.3
	0.03	0.03	5760	2.80E-06	0.8923	89.23

		After 48 hr.				
	Sample	Δw	At	CR	Θ	IE%
L-AgNPs	0	0.35	11520	3E-05	0	0.00
	0.0025	0.19	11520	1.6E-05	0.457	45.71
	0.005	0.15	11520	1.3E-05	0.571	57.14
	0.01	0.09	11520	7.8E-06	0.743	74.29
	0.02	0.08	11520	6.6E-06	0.783	78.29
	0.03	0.05	11520	4.3E-06	0.857	85.71
S-AgNPs	0	0.35	11520	3E-05	0	0.00
	0.0025	0.12	11520	1E-05	0.657	65.71
	0.005	0.11	11520	9.5E-06	0.686	68.57
	0.01	0.09	11520	7.8E-06	0.743	74.29
	0.02	0.07	11520	6.1E-06	0.8	80.00
	0.03	0.06	11520	5.2E-06	0.829	82.86
Z-AgNPs	0	0.35	11520	3E-05	0	0.00
	0.0025	0.16	11520	1.4E-05	0.543	54.29
	0.005	0.14	11520	1.2E-05	0.6	60.00
	0.01	0.12	11520	1E-05	0.657	65.71
	0.02	0.1	11520	8.7E-06	0.714	71.43
	0.03	0.08	11520	4.80E-06	0.84	84

Article in Press

		After 72 hr.				
	Sample	Δw	At	CR	Θ	IE%
L-AgNPs	0	0.45	17280	2.60E-05	0.00	0.00
	0.0025	0.22	17280	1.27E-05	0.51	51.11
	0.005	0.16	17280	9.26E-06	0.64	64.44
	0.01	0.12	17280	6.94E-06	0.73	73.33
	0.02	0.1	17280	5.79E-06	0.78	77.78
	0.03	0.07	17280	4.05E-06	0.84	84.44
S-AgNPs	0	0.45	17280	2.60E-05	0.00	0.00
	0.0025	0.14	17280	8.10E-06	0.69	68.89
	0.005	0.12	17280	6.94E-06	0.73	73.33
	0.01	0.09	17280	4.92E-06	0.81	81.11
	0.02	0.08	17280	4.63E-06	0.82	82.22
	0.03	0.08	17280	4.34E-06	0.83	83.33
Z-AgNPs	0	0.45	17280	2.60E-05	0.00	0.00
	0.0025	0.23	17280	1.33E-05	0.49	48.89
	0.005	0.17	17280	9.84E-06	0.62	62.22
	0.01	0.14	17280	8.10E-06	0.69	68.89
	0.02	0.12	17280	6.94E-06	0.73	73.33
	0.1	17280	5.00E-06	0.8077	80.77	

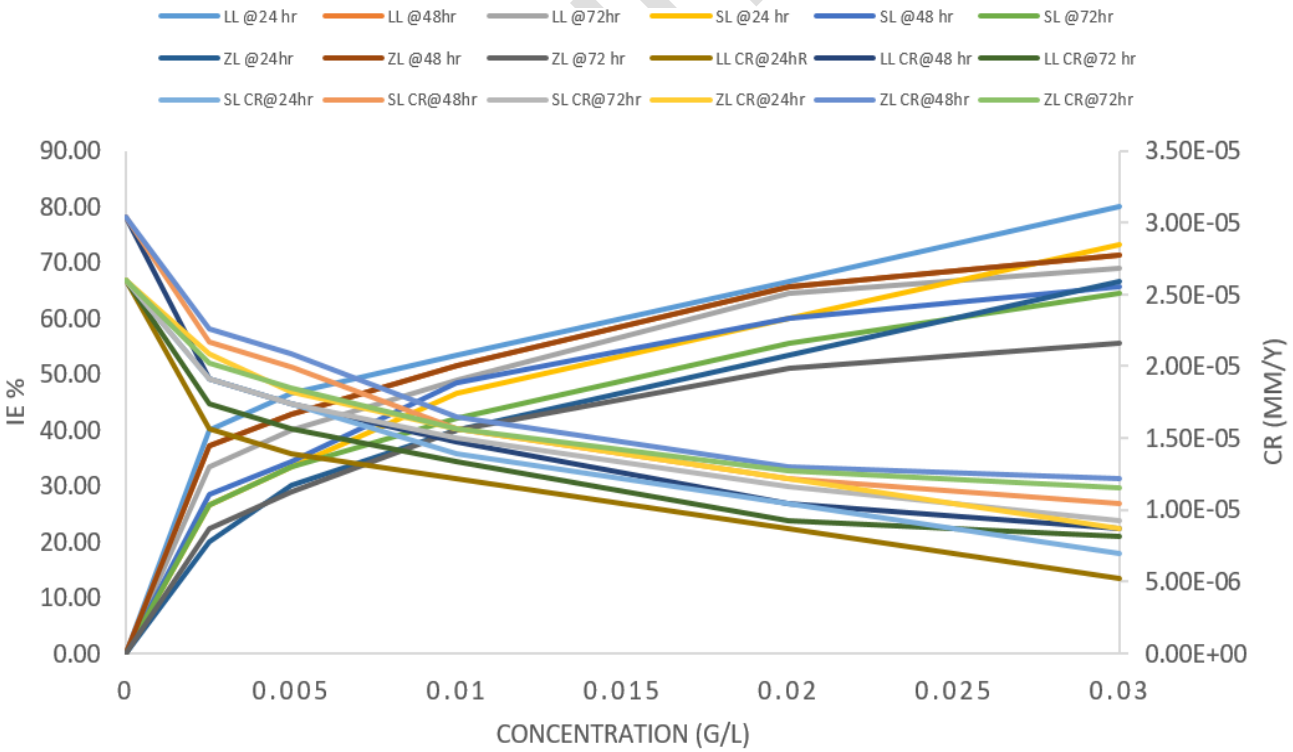

Fig. 9. IE% and corrosion rate vs. concentration relationship for LL, SL, and ZL extracts.

Weight loss studies, Figure 11, demonstrated clear inverse relationship between inhibitor concentration and material degradation. As concentration increased from 0.0025 to 0.03 g/L, inhibition efficiency (IE%) increased

progressively, LL extracts: 72-81% IE%, while; L-AgNPs: 84-94.7% IE% (optimal at 0.03 g/L) AgNPs showed 13-20% superior performance compared to crude extracts at equal mass concentrations, highlighting the enhancement from nanoparticle formation. IE% values plateaued beyond 0.03 g/L, suggesting surface saturation.

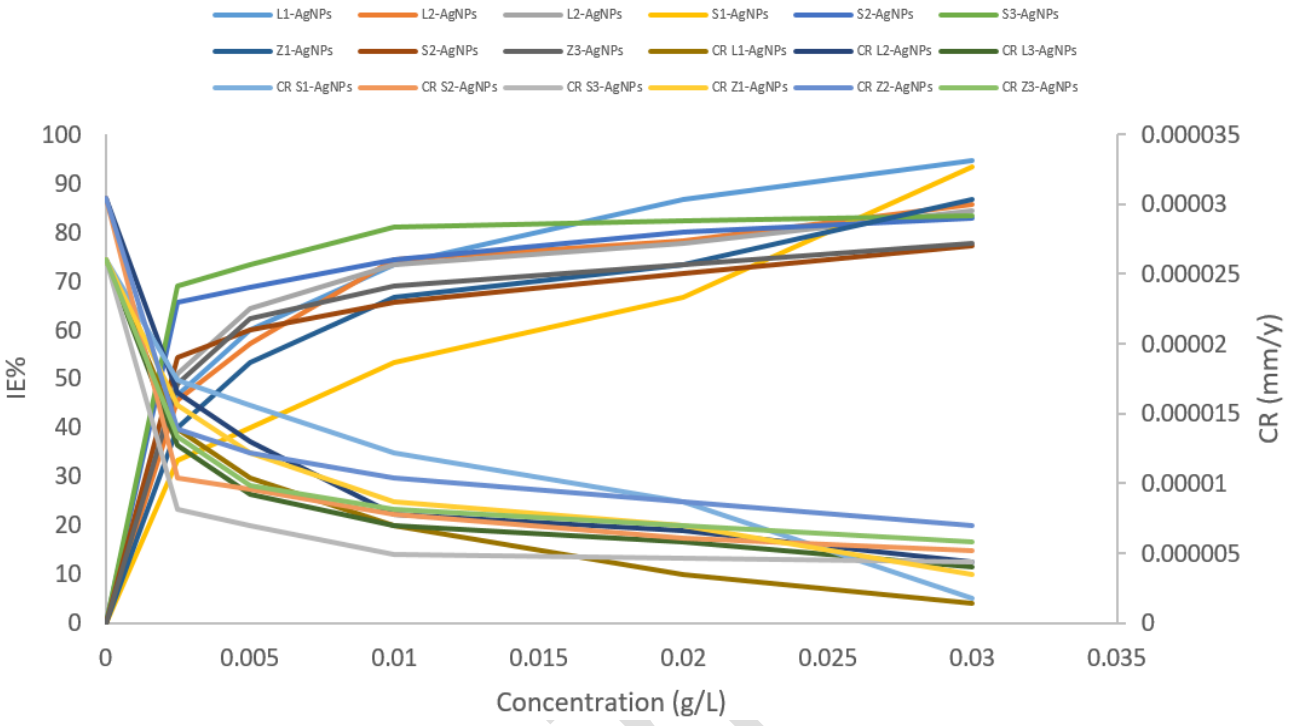

Fig. 10. IE% and corrosion rate vs. concentration relationship for L-AgNPs, S-AgNPs, and Z-AgNPs.

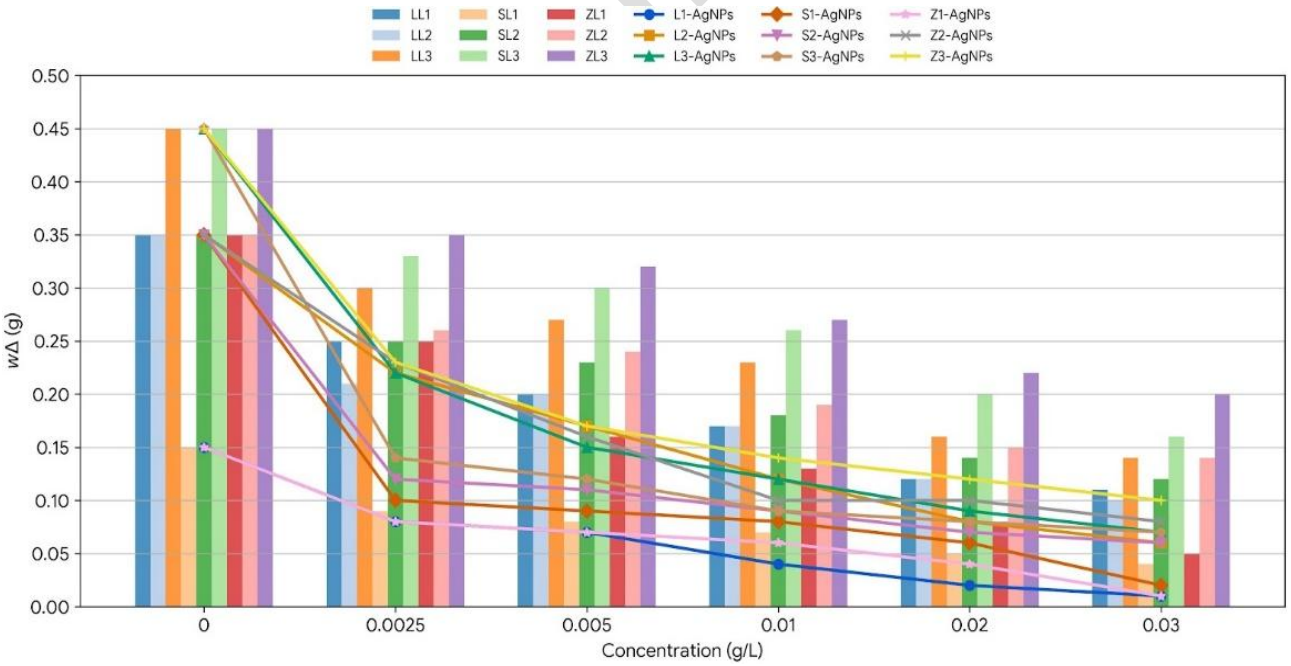

Fig. 11. Weight loss vs. concentration relationship.

Langmuir adsorption isotherm analysis, Figure 12 revealed characteristic linear trends expressed by $C/\theta = (1/K_{ads}) + C$, indicating monolayer adsorption. High correlation coefficients ($R^2 \geq 0.97$) confirmed model validity. Adsorption equilibrium constants (K_{ads}) were particularly high for AgNPs derivatives (Z1-AgNPs: 232.5581), reflecting strong binding affinity with steel surfaces, Figure 12. Thermodynamic parameters, Table 6, was

calculated at 333˚K shows, - ΔG values: -21.29 to -23.12 kJ/mol, which suggest the spontaneous covering and protection of the inhibitor to mild steel surface, which indicate energy-favorable adsorption. - ΔH values: ~-15 kJ/mol, mildly exothermic process). - ΔS values: -0.0162 to -0.0247 kJ/mol·K. The decreased entropy, may be related to organized monolayer formation. These parameters indicate predominantly physisorptive adsorption with possible weak chemisorptive contributions.

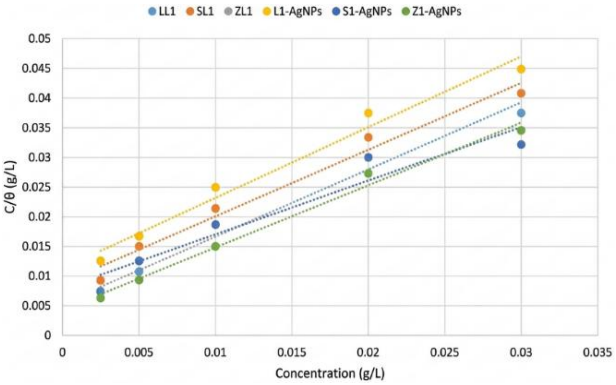

Fig. 12. Langmuir adsorption isotherm.

Open-circuit potential (OCP) monitoring, Figure 13, showed L-AgNPs maintained most stable potential (~-6.5 × 10^{-3} V) throughout 3000 seconds exposure, indicating durable protective film formation. In contrast, SL and ZL extracts showed greater potential fluctuations, suggesting less stable surface films.

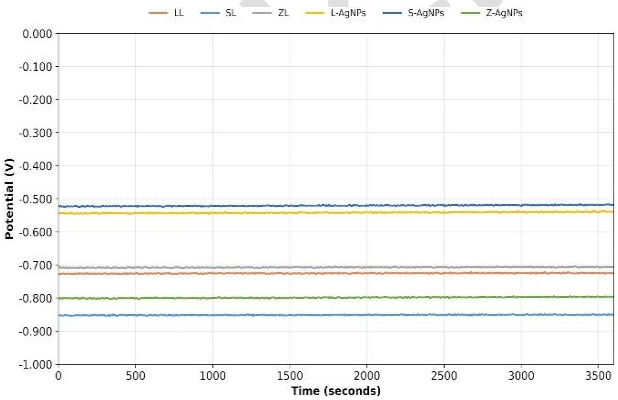

Fig. 13. Variation of potential with time using lillium candidium extracts and their AgNPs.

Tafel polarization curves, Figure 14, revealed that L-AgNPs exhibited lowest Tafel slope (~120 mV/dec), indicating favorable charge-transfer mechanism and enhanced corrosion inhibition compared to S-AgNPs (~150 mV/dec) and Z-AgNPs (~160 mV/dec). Lower slopes correlate with stronger adsorption and more uniform surface coverage.

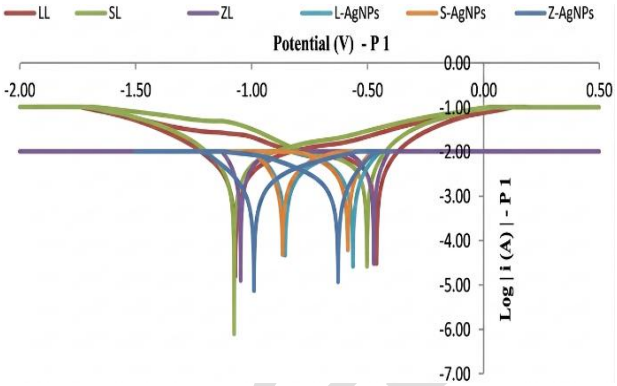

Fig. 14. Variation of current density with potential.

Cyclic voltammetry, Figure 15, confirmed that L-AgNPs produced marked reduction in cathodic current density, reflecting strong suppression of cathodic reactions. The relatively stable and less negative current response across potential range indicates formation of uniform, adherent protective film effectively passivating the mild steel surface.

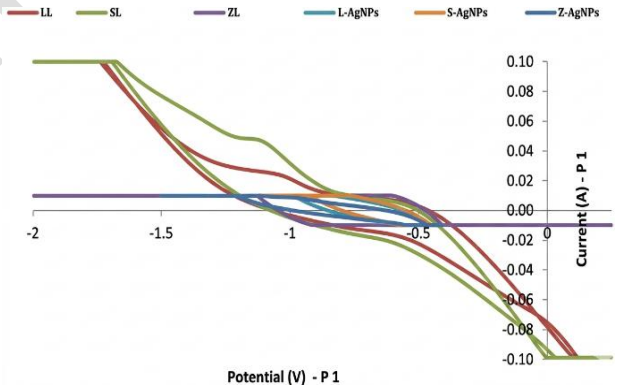

Fig. 15. Cyclic voltammetry of the prepared extracts and their AgNPs.

Our results demonstrate superior performance compared to literature values for green AgNPs corrosion inhibitors, Table 7. L-AgNPs achieved 94.7% IE% compared to typical literature values of 60-90% for plant-based AgNPs. This enhanced performance is attributed to the unique phytochemical profile of Lilium candidum L., particularly the high content of flavonoids and terpenoids, which facilitate efficient silver ion reduction and stable adsorption on steel surfaces.

Article in Press

Table 6. Thermodynamic parameters (Δ H, Δ G, Δ S) and adsorption characteristics of LL1, SL1, ZL1, and their AgNPs derivatives as corrosion inhibitors at 333 K.

Sample	R2	Intercept	K_ads	ΔH	ΔG	ΔS	Type
LL1	0.9773	0.0054	185.1852	-15	-22.81	-0.022	Physisorption (borderline)
SL1	0.9792	0.0088	113.6364	-15	-21.75	-0.0162	Physisorption (borderline)
ZL1	0.9782	0.0112	89.2857	-15	-21.29	-0.0181	Physisorption (borderline)
L1-AgNPs	0.9782	0.0112	89.2857	-15	-21.29	-0.0181	Physisorption (borderline)
S1-AgNPs	0.9246	0.008	125	-15	-21.9	-0.0181	Physisorption (borderline)
Z1-AgNPs	0.99	0.0043	232.5581	-15	-23.12	-0.0247	Physisorption (borderline)

Table 7. Comprehensive data: plant-mediated silver nanoparticles (AgNPs) as corrosion inhibitors.

Plant Source	Metal	Medium	Conc.	Temp.	WL / CR	Max IE (%)	Analysis Methods	Ref.
Lilium candidum L.	Mild steel	Simulated Seawater	3.5 wt.%	333K	CR:1.4E-06	94.7%	Gravimetric, electrochemical (CV, Tafel), and thermodynamics	**Current study**
Anacardium occidentale	Mild Steel	Simulated Seawater	0.3 g/L	40 °C 80 °C	CR: 2.32 mm/yr	90.50% 90.00%	EIS, PDP, SEM, AFM, FTIR	[36]
Nicotiana tabacum	Mild Steel	1.0 N HCl	200 ppm	303-333K	CR: --- WL:10mg/cm^2	98.00%	Gravimetric, EIS, PDP, SEM	[37]
Borassus aethiopum	Mild Steel	1.0 M HCl	400 ppm	25 °C	CR: 2.32 mm/yr	80.60%	Gravimetric, UV-Vis, FTIR	[38]
Citrus reticulata	Mild Steel	1.0 M HCl	100 mg/L	303 K and 333 K	-	93.90% 90.30%	PDP, EIS, SEM, XRD	[39]
Senna occidentalis	Mild Steel	0.5 M H_2SO_4	5 g/dm^3	298 K and 308 K	WL: 0.0087 g	44.16% and 65.60%	Gravimetric, UV-Vis, FTIR	[40]
Garcinia gummi-gutta	Mild Steel	1.0 M HCl	1.5wt% AgNP+epoxy	---	CR: 0.051 mmpy	99.20%	Gravimetric, EIS, SEM, AFM	[41]
Brassaiopsis hainla	Mild Steel	1.0 M HCl	1000 ppm	30 °C	CR: 1.25 mg/cm^2/h	69.59%	EIS, PDP, SEM, EDX, XRD	[42]
Citrus aurantium	Mild Steel	0.5 M HCl	1000 ppm	30 °C	-	70.00%	EIS, PDP, SEM, UV-Vis	[43]
Lonchocarpus laxiflorus	Mild Steel	1.0 M HCl	500 ppm	303K 313K 323K 333K	CR: 0.580 mmpy	80.90 66.00 61.76 60.43	Gravimetric, PDP	[44]

Article in Press

4. CONCLUSION

The findings of this work confirm that Lilium candidum *L.* is an effective and sustainable source for the green synthesis of silver nanoparticles with enhanced antifungal and corrosion inhibition properties. The phytochemical-rich extracts enabled the formation of stable, spherical AgNPs with improved surface activity compared to the corresponding crude extracts.

Corrosion inhibition results clearly demonstrated that both extract type and nanoscale formulation play critical roles in protection efficiency, with leaf-derived systems consistently outperforming stem- and flower-derived counterparts. After 24 h immersion, inhibition efficiencies followed the order LL > SL > ZL (80% > 73% > 67%) for the extracts and L-AgNPs > S-AgNPs > Z-AgNPs (94.7% > 93.3% > 89.23%) for the nanoparticles, highlighting the significant enhancement achieved through nanoparticle synthesis. Increasing inhibitor concentration improved surface coverage and reduced corrosion rates until saturation was reached, while longer immersion times resulted in partial loss of efficiency due to gradual desorption of the protective layer. Adsorption and thermodynamic analyses confirmed spontaneous, predominantly physisorptive monolayer formation, supported by electrochemical and quantum chemical results.

Acknowledgement

I'd like to acknowledge Dr S.M. Siva Kumar, Jazan University, Saudi Arabia for helping in zeta analysis.

REFERENCES

[1] A. Zeino, I. Abdulazeez, M. Khaled, M. W. Jawich, and I. B. Obot, "Mechanistic study of polyaspartic acid (PASP) as eco-friendly corrosion inhibitor on mild steel in 3% NaCl aerated solution," *Journal of Molecular Liquids*, vol. 250, pp. 50–62, Nov. 2017, doi: 10.1016/j.molliq.2017.11.160.

[2] [M. Koundal, C. Sharma, and A. K. Singh, "Effect of organic component (tartrate) addition on cerium nitrate's ability to inhibit corrosion of mild steel in NaCl solution," *Journal of Rare Earths*, vol. 42, no. 10, pp. 1995–2002, Jan. 2024, doi: 10.1016/j.jre.2024.01.011.

[3] M. Ouakki *et al.*, "Comparative study of natural and synthetic polymers as corrosion inhibitors for mild steel in 1.0 M HCl solution," *Colloids and Surfaces a Physicochemical and Engineering Aspects*, vol. 723, p. 137355, May 2025, doi: 10.1016/j.colsurfa.2025.137355.

[4] J. Pan, X. He, and K. Cao, "Electrochemical and theoretical studies of two amino acid ionic liquids as corrosion inhibitors for mild steel in 3.5 wt% NaCl solution," *International Journal of Electrochemical Science*, vol. 20, no. 2, p. 100916, Dec. 2024, doi: 10.1016/j.ijoes.2024.100916.https://doi.org/10.1016/j.ijoes.2024.100916.

[5] A. Chatterjee, S. Sen, S. Singh, S. Bhardwaj, and P. K. Maji, "Corrosion protection of mild steel via cerium nitrate loaded acrylic-vinyl polysilazane based hybrid coatings," *Progress in Organic Coatings*, vol. 197, p. 108831, Sep. 2024, doi: 10.1016/j.porgcoat.2024.108831.

[6] J. Hu and G. Zeng, "Chitosan grafted with gallic acid and cerium dioxide hybrid nanocomposites as environmentally friendly corrosion inhibitors for mild steel: An experimental and computational study," *International Journal of Biological Macromolecules*, vol. 279, no. Pt 2, p. 135074, Sep. 2024, doi: 10.1016/j.ijbiomac.2024.135074.

[7] H. Kahkesh and B. Zargar, "Designing a novel and eco-friendly organic/inorganic system for mild steel corrosion protection in saline environment: Electrochemical and surface studies," *Journal of Industrial and Engineering Chemistry*, vol. 146, pp. 603–620, Dec. 2024, doi: 10.1016/j.jiec.2024.11.044.

[8] M. M. Solomon, H. Gerengi, and S. A. Umoren, "Carboxymethyl Cellulose/Silver Nanoparticles Composite: Synthesis, characterization and application as a benign corrosion inhibitor for ST37 steel in 15% H2SO4Medium," *ACS Applied Materials & Interfaces*, vol. 9, no. 7, pp. 6376–6389, Jan. 2017, doi: 10.1021/acsami.6b14153.

[9] T. Asafa *et al.*, "Inhibition efficiency of silver nanoparticles solution on corrosion of mild steel, stainless steel and aluminum in 1.0 M HCl medium," *IOP Conference Series Materials Science and Engineering*, vol. 805, no. 1, p. 012018, Mar. 2020, doi: 10.1088/1757-899x/805/1/012018.

[10] M. Zaccai *et al.*, "Medicinal Properties of Lilium candidum L. and Its Phytochemicals," *Plants*, vol. 9, no. 8, p. 959, Jul. 2020, doi: 10.3390/plants9080959.

[11] A. Vachálková, E. Eisenreichová, M. Haladová, P. Mucaji, B. Józová, and L. Novotný, "Potential carcinogenic and inhibitory activity of compounds isolated from *Lilium candidum* L.," *Neoplasma*, vol. 47, no. 5, pp. 313–318, 2000.

[12] J. Patocka, "Bioactivity of Lilium candidum L : A Mini Review," *Biomedical Journal of Scientific & Technical Research*, vol. 18, no. 5, Jun. 2019, doi: 10.26717/bjstr.2019.18.003204.

[13] S. Revathi *et al.*, "Green synthesis and characterization of silver nanoparticles (AgNP) using Acacia nilotica plant extract and their anti-bacterial activity," *Food Chemistry Advances*, vol. 4, p. 100680, May 2024, doi: 10.1016/j.focha.2024.100680.

Article in Press

[14] J. Yadav and P. Chauhan, "Green synthesis of silver nanoparticles using Citrus X sinensis (Orange) fruit extract and assessment of their catalytic reduction," *Materials Today Proceedings*, vol. 62, pp. 6177–6181, Jan. 2022, doi: 10.1016/j.matpr.2022.05.041.

[15] M. Rizwan and C. Gwenin, "Nanomaterials in renewable energy: UV-Visible spectroscopy characterization and applications," in *Elsevier eBooks*, 2021, pp. 103–120. doi: 10.1016/b978-0-12-821709-2.00017-7.

[16] N. G. Tosun and A. Özgür, "Synthesis methods and characterization parameters of silver nanoparticles," in *Elsevier eBooks*, 2024, pp. 39–65. doi: 10.1016/b978-0-443-15343-3.00005-x.

[17] N. Ahmad, M. A. Ansari, A. Al-Mahmeed, R. M. Joji, N. K. Saeed, and M. Shahid, "Biogenic silver nanomaterials synthesized from Ocimum sanctum leaf extract exhibiting robust antimicrobial and anticancer activities: Exploring the therapeutic potential," *Heliyon*, vol. 10, no. 15, p. e35486, Jul. 2024, doi: 10.1016/j.heliyon.2024.e35486.

[18] H. K. Permatasari *et al.*, "Green synthesized Moringa oleifera Leaf Powder – Silver Nanoparticles (MOLP-AgNPs) promotes apoptosis by targeting Caspase-3 and Phosphorylated-AKT signaling in MCF-7 cells," *Journal of Agriculture and Food Research*, vol. 19, p. 101640, Jan. 2025, doi: 10.1016/j.jafr.2025.101640.

[19] D. D. C. S. Batista *et al.*, "Effectiveness of Aloe vera (L.) Burm.F. biomembranes with silver nanoparticles in the clinical experimental treatment of skin lesions of dogs with leishmaniasis," *Microbial Pathogenesis*, vol. 206, p. 107759, May 2025, doi: 10.1016/j.micpath.2025.107759.

[20] A. Dashora, K. Rathore, S. Raj, and K. Sharma, "Synthesis of silver nanoparticles employing Polyalthia longifolia leaf extract and their in vitro antifungal activity against phytopathogen," *Biochemistry and Biophysics Reports*, vol. 31, p. 101320, Aug. 2022, doi: 10.1016/j.bbrep.2022.101320.

[21] A. Dashora, K. Rathore, S. Raj, and K. Sharma, "Synthesis of silver nanoparticles employing Polyalthia longifolia leaf extract and their in vitro antifungal activity against phytopathogen," *Biochemistry and Biophysics Reports*, vol. 31, p. 101320, Aug. 2022, doi: 10.1016/j.bbrep.2022.101320.

[22] B. P. Kafle, "Introduction to nanomaterials and application of UV–Visible spectroscopy for their characterization," in *Elsevier eBooks*, 2019, pp. 147–198. doi: 10.1016/b978-0-12-814866-2.00006-3.

[23] J. R. Shaikh and M. Patil, "Qualitative tests for preliminary phytochemical screening: An overview," *International Journal of Chemical Studies*, vol. 8, no. 2, pp. 603–608, Mar. 2020, doi: 10.22271/chemi.2020.v8.i2i.8834.

[24] M. Megawati, M. Yuwono, and R. Primaharinastiti, "Antibacterial activity of Randu Honey against some bacterial pathogens using agar well diffusion method," *Riset Informasi Kesehatan*, vol. 14, no. 1, p. 49, Jan. 2025, doi: 10.30644/rik.v14i1.954.

[25] N. Setti *et al.*, "Structural effect of bipyrazole derivatives on corrosion inhibition of carbon steel in 1 M HCl: weight loss, electrochemical measurements, XPS/SEM surface analysis, DFT and MC simulations," *Physical Chemistry Chemical Physics*, vol. 27, no. 10, pp. 5371–5394, Jan. 2025, doi: 10.1039/d4cp02946a.

[26] A. Tomar, A. M. Khan, G. Ji, R. Haldhar, E. Berdimurodov, and A. Sarkar, "Investigation on corrosion inhibition characteristics of (1Z,4Z)-N′1, N′4-bis(4-methoxyphenyl) succinimidohydrazide for mild steel in 1.0 M HCl by weight loss measurements, surface imaging, and computational analysis," *Canadian Metallurgical Quarterly*, vol. 65, no. 1, pp. 650–662, Apr. 2025, doi: 10.1080/00084433.2025.2492451.

[27] ASTM International, *ASTM G31-21R25: Standard Practice for Laboratory Immersion Corrosion Testing of Metals*, West Conshohocken, PA, USA, 2025. doi: 10.1520/G0031-21R25.

[28] ASTM International, *ASTM G59-23: Standard Test Method for Conducting Potentiodynamic Polarization Resistance Measurements*, West Conshohocken, PA, USA, 2023. doi: 10.1520/G0059-23.

[29] S. Rauch *et al.*, "Highly specific SARS-CoV-2 main protease (Mpro) mutations against the clinical antiviral ensitrelvir selected in a safe, VSV-based system," *Antiviral Research*, vol. 231, p. 105969, Jul. 2024, doi: 10.1016/j.antiviral.2024.105969.

[30] J. W. Soedarsono, A. Andoko, K. Diharjo, F. Gapsari, S. M. Rangappa, and S. Siengchin, "Biodegradable PLA/HEC-ZNO Nanocomposite for corrosion protection of ASTM A36 steel: A combined quantum and electrochemical analysis," *Case Studies in Chemical and Environmental Engineering*, vol. 11, p. 101039, Dec. 2024, doi: 10.1016/j.cscee.2024.101039.

[31] A. A. Al-Amiery, L. M. Shaker, A. A. H. Kadhum, and Takriff, "Corrosion Inhibition of Mild Steel in Strong Acid Environment by 4-((5,5-dimethyl-3-oxocyclohex-1-en-1-yl)amino)benzenesulfonamide," *Tribology in Industry*, vol. 42, no. 1, pp. 89–101, Mar. 2020, doi: 10.24874/ti.2020.42.01.09.

Article in Press

[32] J. R. Shaikh and M. Patil, "Qualitative tests for preliminary phytochemical screening: An overview," *International Journal of Chemical Studies*, vol. 8, no. 2, pp. 603–608, Mar. 2020, doi: 10.22271/chemi.2020.v8.i2i.8834.

[33] P. S. Kalsi, *Spectroscopy of Organic Compounds*, 6th ed. New Delhi, India: New Age International (P) Limited, 2017.

[34] C. V. Vivas *et al.*, "Interactions Between Silver Nanoparticles and Culture Medium Biomolecules with Dose and Time Dependencies," *Journal of Fluorescence*, vol. 35, no. 2, pp. 835–854, Jan. 2024, doi: 10.1007/s10895-023-03564-x.

[35] W. Abdussalam-Mohammed, K. Edbey, H. E. Farhat, P. Shah, S. S. Shamsi, and A. Bhattarai, "Facile green synthesis of novel AgNPs using Hyoscyamus leaf extract as capping agent: Characterization and their potential antibacterial activities," *Inorganic Chemistry Communications*, vol. 173, p. 113893, Jan. 2025, doi: 10.1016/j.inoche.2025.113893.

[36] A. O. Ezzat, V. S. Aigbodion, H. A. Al-Lohedan, and C. J. Ozoude, "Unveiling the corrosion inhibition efficacy and stability of silver nanoparticles synthesized using Anacardium occidentale leaf extract for mild steel in a simulated seawater solution," *RSC Advances*, vol. 14, no. 26, pp. 18395–18405, Jan. 2024, doi: 10.1039/d4ra02362e.

[37] S. R. Al-Mhyawi, "Green synthesis of silver nanoparticles and their inhibitory efficacy on corrosion of carbon steel in hydrochloric acid solution," *International Journal of Electrochemical Science*, vol. 18, no. 9, p. 100210, May 2023, doi: 10.1016/j.ijoes.2023.100210.

[38] A.-L. Usman, "Eco-Friendly Synthesis of Silver Nanoparticles from African Fan Palm (Borassus aethiopum) Leaf Extract for Corrosion Inhibition of Mild Steel in 1 M HCl," *Journal of Science Innovation and Technology Research*, Dec. 2025, doi: 10.70382/ajsitr.v10i9.058.

[39] E. Ituen, E. Ekemini, L. Yuanhua, and A. Singh, "Green synthesis of Citrus reticulata peels extract silver nanoparticles and characterization of structural, biocide and anticorrosion properties," *Journal of Molecular Structure*, vol. 1207, p. 127819, Jan. 2020, doi: 10.1016/j.molstruc.2020.127819.

[40] V. O. Egbeneje, S. E. Okhale, C. Imoisi, I. O. Ogbogo, and O. Ojo, "Evaluation of the Inhibitive Properties of Silver Nanoparticles in Senna occidentalis Root Extract as Corrosion Inhibitor of Mild Steel," *Tanzania Journal of Science*, vol. 49, no. 3, pp. 655–663, Sep. 2023, doi: 10.4314/tjs.v49i3.9.

[41] G. K. Shamnamol, S. John, and J. M. Jacob, "Exploring the Corrosion Inhibition Efficacy of Epoxy Merged Silver Nanoparticle Synthesized Using Garcinia gummi-gutta Leaf Extract Against Mild Steel in an Acidic Medium," *Journal of Bio- and Tribo-Corrosion*, vol. 9, no. 4, Oct. 2023, doi: 10.1007/s40735-023-00802-4.

[42] S. Budhathoki *et al.*, "Green synthesis of silver nanoparticles from Brassaiopsis hainla extract for the evaluation of antibacterial and anticorrosion properties," *Heliyon*, vol. 10, no. 15, p. e35642, Aug. 2024, doi: 10.1016/j.heliyon.2024.e35642.

[43] Z. K. Hamze, M. Faraj, R. Mhanna, G. Younes, and M. H. El-Dakdouki, "Corrosion Inhibition Efficiency of Biosynthesized Silver Nanoparticles Using Citrus aurantium Peels Extract," *Journal of Bio- and Tribo-Corrosion*, vol. 10, no. 3, Jun. 2024, doi: 10.1007/s40735-024-00854-0.

[44] [G. Ijuo, N. Surma, and J. Igoli, "Ag-nanoparticles Mediated by Lonchocarpus laxiflorus Stem Bark Extract as Anticorrosion Additive for Mild Steel in 1.0 M HCl Solution," *Prog. Chem. Biochem. Res.*, vol. 5, no. 2, May 2022, doi: 10.22034/pcbr.2022.324366.1208.

Article in Press